CARBON 49 (2011) 2917–2925

available at www.sciencedirect.com

ScienceDirect

journal homepage: www.elsevier.com/locate/carbon

Graphene and nanostructured MnO_2 composite electrodes for supercapacitors

Qian Cheng [a,b], Jie Tang [a,b,*], Jun Ma [a], Han Zhang [a], Norio Shinya [a], Lu-Chang Qin [c,*]

[a] National Institute for Materials Science, 1-2-1 Sengen, Tsukuba 305-0047, Japan
[b] Doctoral Program in Materials Science and Engineering, University of Tsukuba, 1-1-1 Tennodai, Tsukuba 305-8577, Japan
[c] Department of Physics and Astronomy, University of North Carolina at Chapel Hill, Chapel Hill, NC 27599-3255, USA

ARTICLE INFO

Article history:
Received 16 September 2010
Accepted 28 February 2011
Available online 9 March 2011

ABSTRACT

Graphene-based materials are promising electrodes for supercapacitors, owing to their unique two-dimensional structure, high surface area, remarkable chemical stability, and electrical conductivity. In this paper, graphene is explored as a platform for energy storage devices by decorating graphenes with flower-like MnO_2 nanostructures fabricated by electrodeposition. The as-prepared graphene and MnO_2, which were characterized by scanning electron microscopy (SEM) and transmission electron microscopy (TEM), have been assembled into an asymmetric supercapacitor. The specific capacitance of the graphene electrode reached 245 F/g at a charging current of 1 mA after an electro-activation process. This value is more than 60% larger than the one before electro-activation. The MnO_2 nano-flowers which consisted of tiny rods with a thickness of less than 10 nm were coated onto the graphene electrodes by electrodeposition. The specific capacitance after the MnO_2 deposition is 328 F/g at the charging current of 1 mA with an energy density of 11.4 Wh/kg and 25.8 kW/kg of power density. This work suggests that our graphene-based electrodes are a promising candidate for the high-performance energy storage devices.

1. Introduction

In the past few years, considerable efforts have been devoted to develop new energy storage devices with high energy and high power density that can be used in hybrid vehicles and/or electric cars to meet the requirement of low CO_2 emissions. Supercapacitors, which are also called ultracapacitors or electrochemical double layer capacitors, are a kind of promising energy saving devices. They can provide a huge amount of energy in a short period of time, making them indispensable for certain power delivery systems [1]. It is more suitable for energy storage systems due to their excellent cyclability and very good power performance comparing with the conventional batteries. However, supercapacitors often suffer from low energy performance which is usually evaluated by the specific capacitance and energy density. It is therefore necessary to improve their energy performance to meet the higher requirements of future energy storage systems, ranging from portable electronics to hybrid vehicles and large industrial equipment.

The major material components of supercapacitors can be divided into three categories. The first category is carbon materials, such as activated carbon [2,3], carbon nanotubes [4], and graphene [5–7]. The desire for using carbon materials is based on the mechanism of double-layer capacitance. They store the charges electrostatically using reversible adsorption of ions of the electrolyte onto active materials that are electrochemically stable and have a high accessible surface area. The second category is redox-based electrochemical capacitors, where transition metal oxides, such as MnO_2 and RuO_2

* Corresponding authors at: National Institute for Materials Science, 1-2-1 Sengen, Tsukuba 305-0047, Japan (J. Tang).
E-mail addresses: tang.jie@nims.go.jp (J. Tang), lcqin@physics.unc.edu (L.-C. Qin).
0008-6223/$ - see front matter
doi:10.1016/j.carbon.2011.02.068

[8–11], are used for fast and reversible redox reactions at the surface of active materials. But metal oxides usually have a high electrical resistance resulting in a low power density. The third category is conductive polymers, such as polyaniline and polypyrrole [12–15], which have shown high gravimetric and volumetric pseudo-capacitance using various aqueous and nonaqueous electrolytes. However, when used as bulk materials, conducting polymers suffer from a limited stability during cycling that reduces the initial performance [16].

Although activated carbon has a high specific surface area, the low electrical conductivity of activated carbon is limiting its applications in high power density supercapacitors [17]. For example, a commercial activated carbon for supercapacitors can only achieve a specific capacitance of 26 F/g in an organic electrolyte in our tests. Carbon nanotubes (CNTs), with an excellent electrical conductivity and high surface area, have also been studied to replace activated carbon for supercapacitors. However, CNT-based supercapacitors showed a relatively low energy density in our studies and have not met the expected performance.

Graphene, the parent of all graphitic structures ranging from graphite to carbon nanotubes and fullerites, has become one of the most exciting topics of research in the last few years [18]. This two-dimensional material constitutes a new type of nanostructured carbon comprising a single layer of carbon atoms arranged in the graphitic sp^2 bonding configuration. It is distinctly different from CNTs and fullerenes and exhibits many unique properties which have fascinated the scientific as well as the technological community. Graphene and chemically modified graphene sheets have shown a high electrical conductivity [19], high surface area, and good mechanical properties comparable with or even better than CNTs [20]. In addition, graphene-based materials can be easily obtained by simple chemical processing of graphite [21]. Moreover, a graphene-based composite material with individual graphene sheets usually does not depend on the distribution of pores in its solid support to offer its large surface area, rather every chemically modified graphene sheet can "move" physically to adjust to the different types of electrolytes. Therefore, the access to the very high surface area of graphene-based materials by the electrolyte can be maintained while preserving the overall high electrical conductivity of the network [6,22,23].

Transition metal oxides have also been widely studied for use as electrode materials of supercapacitors. Although RuO_2 has exhibited prominent capacitive properties as a supercapacitor electrode material, its high production cost will exclude it from wide and commercial applications. Instead, relatively low-cost materials, such as manganese oxide and nickel oxide, have been explored as the electrode materials, but their power performance is still relatively low, because these metal oxides usually have a low electrical conductivity [24,25]. Among the promising metal oxides, MnO_2 can form many polymorphs such as α-, β-, γ-, and δ-type, offering distinctive properties and wide applications as catalysts, ion-sieves, and especially as an electrode material in Li/MnO_2 and Zn/MnO_2 batteries [26–28]. On the other hand, MnO_2 appears to be a promising material for pseudocapacitors due to its superior electrochemical performance, environmental friendliness, and lower production cost [29–33]. Over the past few years, various nanostructured MnO_2, including dendritic clusters, nanocrystals with different morphologies including nanowires, nanotubes, nanobelts, and nanoflowers, have been successfully synthesized and characterized [34–39]. For example, Yan et al. used the reduction of permanganate by surface carbon to prepare graphene/MnO_2 composite electrodes with necessary binder and conductor agents and obtained specific capacitance of 310 F/kg at the scan rate of 2 mV/s [40]. While this manuscript being under review, it was also brought to our attention of the work by Wu et al. [41], who reported their results of using graphene–MnO_2 composites as electrodes for supercapacitors.

To exploit the potential of graphene-based materials for supercapacitor applications, in this work, we have coated active materials on the graphene sheet to obtain hybrid electrodes for the supercapacitors to further increase the specific capacitance as well as the energy density while maintaining its good power performance. We have fabricated graphene/MnO_2 composite electrodes by in situ anodic electrodeposition of MnO_2 on the graphene electrode. This technique can easily control the coating mass, thickness, uniformity, and morphology of the metal oxide film by simply adjusting the applied current, bath chemistry, and temperature. In addition, we can use this method for an in situ deposition of the metal oxide film, which does not require any additional processing step of adding binders (PTFE) and electric conductors (carbon black or acetylene black). The electrode materials synthesized by chemical routes need to add conductors and binders to make an electrode. Furthermore, our technique can easily synthesize nanostructures which could provide a high surface area, short diffusion path in host material, and good pore structure for the access of electrolyte. We have also designed and assembled an asymmetric supercapacitor system with a graphene electrode as anode and MnO_2-coated graphene as cathode. The graphene/MnO_2 composite electrode has been characterized by scanning electron microscopy, electron diffraction, and high-resolution transmission electron microscopy to understand its morphology and structure. The graphene-based supercapacitor has also been evaluated by cyclic voltammetry (CV), charging and discharging, and electrochemical impedance spectroscopy (EIS) to reveal its electrochemical performance, including specific capacitance, energy density, and power density.

2. Experimental

2.1. *Graphene oxide*

Graphene oxide was synthesized by using a modified Hummers method from graphite in our experiment. Graphite (3.0 g) and $NaNO_3$ (1.5 g) were first mixed together in a flask before 100 ml H_2SO_4 (95%) was added to the flask, which was kept and stirred in an ice bath. Potassium permanganate (8.0 g) was then added to the suspension little by little to avoid overheating. The mixture was stirred at room temperature for 2 h. The color of the suspension would become bright brown. Then, 90 ml of distilled water was added. The temperature of the suspension would reach quickly to about 90 °C and the

color would change to yellow. The diluted suspension was stirred 98 °C for 12 h and 30 ml of 30% H_2O_2 was added to the mixture. For purification, the mixture was washed by rinsing with 5% HCl and then demonized water for several times. After that the suspension was centrifuged at 4000 rpm for 6 min. After filtration and drying in vacuum, graphene oxide was obtained in the form of black powders.

2.2. Reduction of graphene oxide

Graphene oxide (100 mg) was first dispersed in 30 ml distilled water and sonicated for 30 min. Then the suspension was heated to 100 °C and 3 ml hydrazine hydrate was added into the suspension. The suspension was then kept at 98 °C for 24 h. After that the reduced graphene was collected by filtration in the form of black powders. The obtained material was then washed using distilled water for several times to remove the excessive hydrazine and was redistribute into water for sonication. Then the suspension is centrifuged at 4000 rpm for 3 min to remove bulk graphite. The final product was collected by vacuum filtration and dried in vacuum.

2.3. In situ MnO_2 electrodeposition

MnO_2 nanostructures were anodically electrodeposited from a mixture of two different types of solutions (0.1 M Na_2SO_4 and 0.1 $Mn(CH_3COO)_2$) onto the graphene film of dimensions 20×10 mm using a cyclic voltammetric technique (250 mV/s at different cycles). A platinum sheet of 20×10 mm was placed vertically 20 mm away from the working electrode as a counter electrode. An Ag–AgCl plate was used as a reference electrode. Before anodic electrodeposition, the graphene film was cleaned with acetone and then distilled water. After electrodeposition the working electrode was rinsed in distilled water, dried at 60 °C for 1 h in oven to remove any residual water and then stored in a vacuum desiccator. The mass of the manganese oxide deposited on the graphene film was determined from the weight difference between the electrode before and after anodic deposition by using a high precision microbalance. The specific deposit mass was controlled to be 0.2–0.5 mg cm^{-2} depending on the coating cycles.

2.4. Fabrication of test cells

After the graphene and nanostructured MnO_2 materials were obtained, a graphene-based supercapacitor was assembled for evaluation. The fabrication process is shown in Fig. 1. The graphene powders were dispersed in distilled water with a concentration of 0.3 mg/ml and we used a laser pen to observe the Dyndall effect. Then the whole suspension was made into a graphene paper by vacuum filtering. After that the graphene paper is cut into pieces of specific dimensions as electrodes and ready for anodic MnO_2 electrodeposition. The MnO_2 coated graphene is then assembled with the graphene electrode into the two-electrode configuration for testing. The anode is made of pure graphene and cathode is made of the MnO_2-coated graphene. Both of the two electrodes were using a high purity titanium sheet as current collector. The two electrodes were separated by a thin polypropylene film in a 1 M KCl aqueous electrolyte solution.

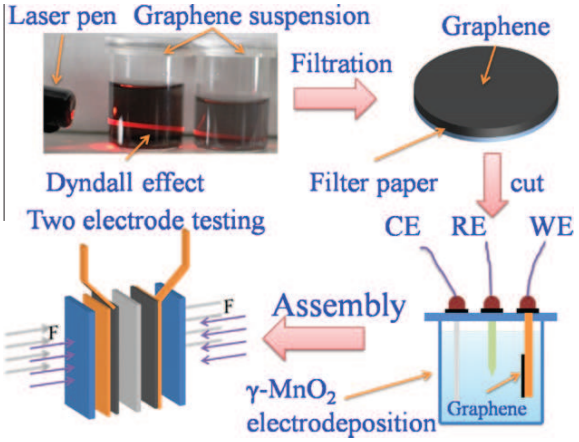

Fig. 1 – Illustrative fabrication process of the composite electrode. The graphene was first suspended in distilled water. Then the whole suspension was made into a graphene paper by vacuum filtering, after which the graphene paper is cut into pieces of designed dimensions for anodic MnO_2 electrodeposition as electrode. The MnO_2 coated graphene is then assembled with the graphene electrode for two-electrode test.

2.5. Electrochemical measurement

The electrochemical properties and capacitance of the supercapacitor electrodes were studied in the two-electrode system by cyclic voltammetry (CV) and electrochemical impedance spectroscopy (EIS). The CV response of the electrodes was measured at different scan rates varying from 10 to 100 mV/s. The voltammetric testing was carried out at potentials between 0 and 0.9 V in a 1 M KCl aqueous electrolyte solution. Impedance spectroscopy measurements were carried out without DC bias sinusoidal signal of 0.005 V over the frequency range from 10 kHz to 0.1 Hz.

2.6. Structural characterization

The morphologies and nano-scale structure of graphene and manganese oxide were examined using scanning electron microscopy (SEM, JSM-6500) and transmission electron microscopy (TEM, JEM-2100).

3. Results and discussion

3.1. Morphology of graphene and MnO_2-coated graphene

Fig. 2 shows the morphologies of the as-synthesized graphene oxide and graphene. Fig. 2a is an SEM image of our synthesized graphene oxide (GO), from which thin sheets are revealed. Fig. 2b is an SEM image of the sample after chemical reduction and the graphene showed morphologies like wrinkled paper. A TEM image of the as-synthesized graphene is shown in Fig. 2c. In this particular case, there are two few-layer graphene sheets overlapped. The inset image is an electron diffraction pattern of the graphene sheets. A few typical first order and second order Bragg reflections are also indi-

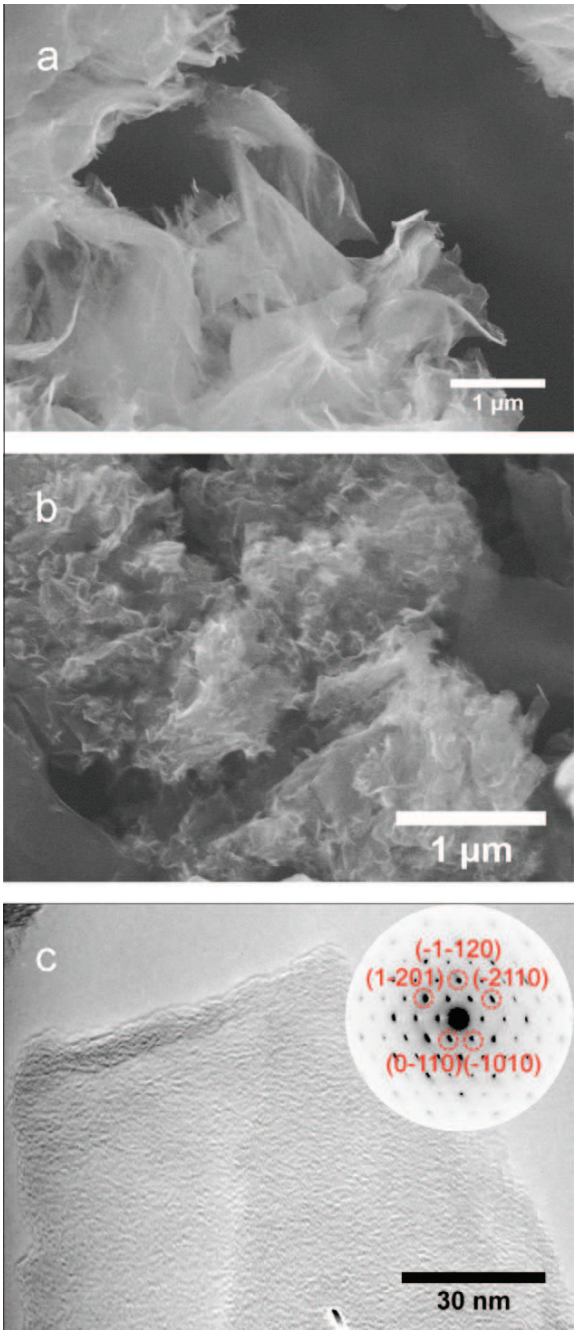

Fig. 2 – Morphology of graphene oxide and graphene. (a) SEM image of graphene oxide, (b) SEM image of graphene, and (c) TEM image of graphene sheets in high magnification. The inset is an electron diffraction pattern of the graphene nanosheets where a few typical Bragg reflections are also indexed.

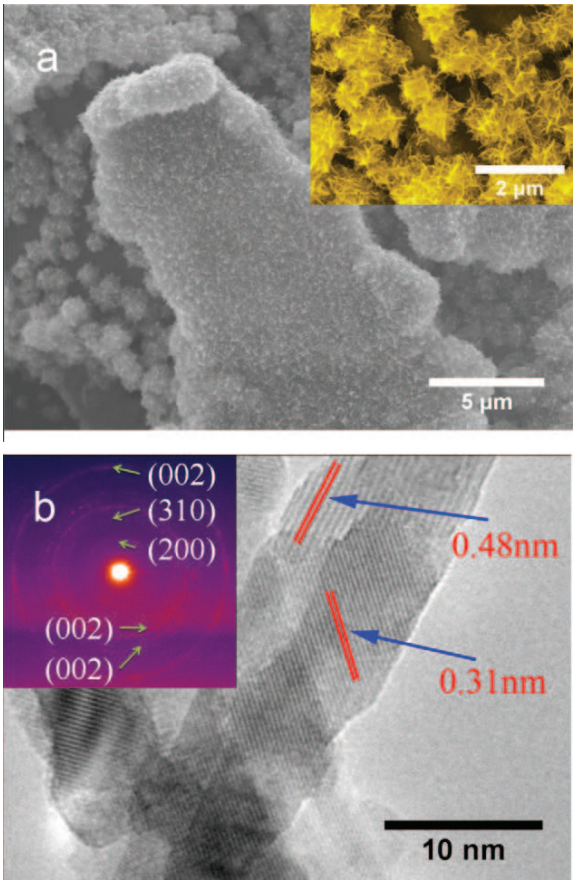

Fig. 3 – Morphology and structural characterization of as-coated MnO_2 graphene. (a) SEM image of MnO_2 nanoflowers. The inset is a portion of the image at higher magnification, revealing that the MnO_2 nanoflowers are made of tiny nanorods. (b) High resolution TEM image of the MnO_2 nanoflowers/nanorods. The inset is an electron diffraction pattern of the MnO_2 nanoflowers.

cated with their Miller indices assigned. Though the TEM image showed an amorphous-like morphology, the corresponding electron diffraction pattern demonstrated clearly the excellent crystallinity of the graphene sheets.

The morphology of the as-synthesized MnO_2 nanostructures is shown in Fig. 3. Fig. 3a is an SEM image of the MnO_2 nanoflowers coated on the graphene film. The graphene was not seen directly in the image due to high-density coating of MnO_2. We can also observe from the low magnification image (Fig. 3a) that the MnO_2 nanoflowers grew on all surfaces of the graphene film. When examined at a higher resolution, as shown in the inset of Fig. 3a, we saw that the MnO_2 nanoflowers were actually composed of a lot of tiny nanorods. The as-synthesized MnO_2 nanorods have a typical diameter of less than 10 nm and the structure of the nanorods is γ-MnO_2 as confirmed by high-resolution electron microscopy (HREM) and electron diffraction (Fig. 3b). The MnO_2 nanosructures synthesized here may have preferably grown on the energetically favorable sites under the cyclic voltammetric control, resulting in a highly porous structure that promotes efficient contacts between the active material and the electrolyte, providing more active sites for electrochemical reactions. It should also be noted that structures with porosity and interconnectivity supply additional accessible space for ions while maintaining sufficient conductivity for solid-state electronic transfer. Moreover, the rod-like structure can provide short

diffusion path lengths to both ions and electrons and also sufficient porosity for electrolyte penetration giving rise to high charging and discharging rates [42].

3.2. *Electrochemical behavior of graphene and MnO_2-coated graphene electrodes*

Fig. 4a shows cyclic voltammetric (CV) loops of a pure graphene supercapacitor electrode with various scan rates in the range of 10–100 mV/s. As we know, the shape of the CV loops of a supercapacitor should be rectangular provided that there is a low contact resistance and larger resistance distorts the loop, resulting in a narrower loop with an oblique angle as observed. The CV curves of our device are close to rectangular at the applied scan rates including the high scan rate of 100 mV/s, indicating an excellent capacitive behavior and a low contact resistance in the supercapacitor. The charge and discharge curves at different charging current are shown in Fig. 4b. The apparent surface area of the electrode is 2 cm^2. The discharge curves are almost linear in the total range of potential, which shows a very good capacitive behavior [43].

Using the above measured experimental data, we have calculated the single electrode capacitance – it is twice the total capacitance C in the two electrode system. The capacitance is 150 F/g, and the maximum storage energy is also calculated as 5.2 Wh/kg.

There is a very interesting phenomenon that we observed in the galvanostatic charge and discharge under 4 mA for about 1300 cycles. The specific capacitance did not decrease but actually increased dramatically as shown in Fig. 4c and this process is termed electro-activation in the present work. A highly possible reason is that the graphene sheets can move to adjust to the different electrolyte ions. The long time charging and discharging may also help the ions accessing fully the graphene sheets to take full advantages of the surface area. For the few-layered graphene sheets, they tend to aggregate to become thicker. However, the long activation can let the ions in the electrolyte intercalate into the spaces between the graphene layers and therefore, producing more surface area for the ions to access to. This is attributed to the observation of increasing specific capacitance. We also immersed the whole test cell in the electrolyte for the same duration

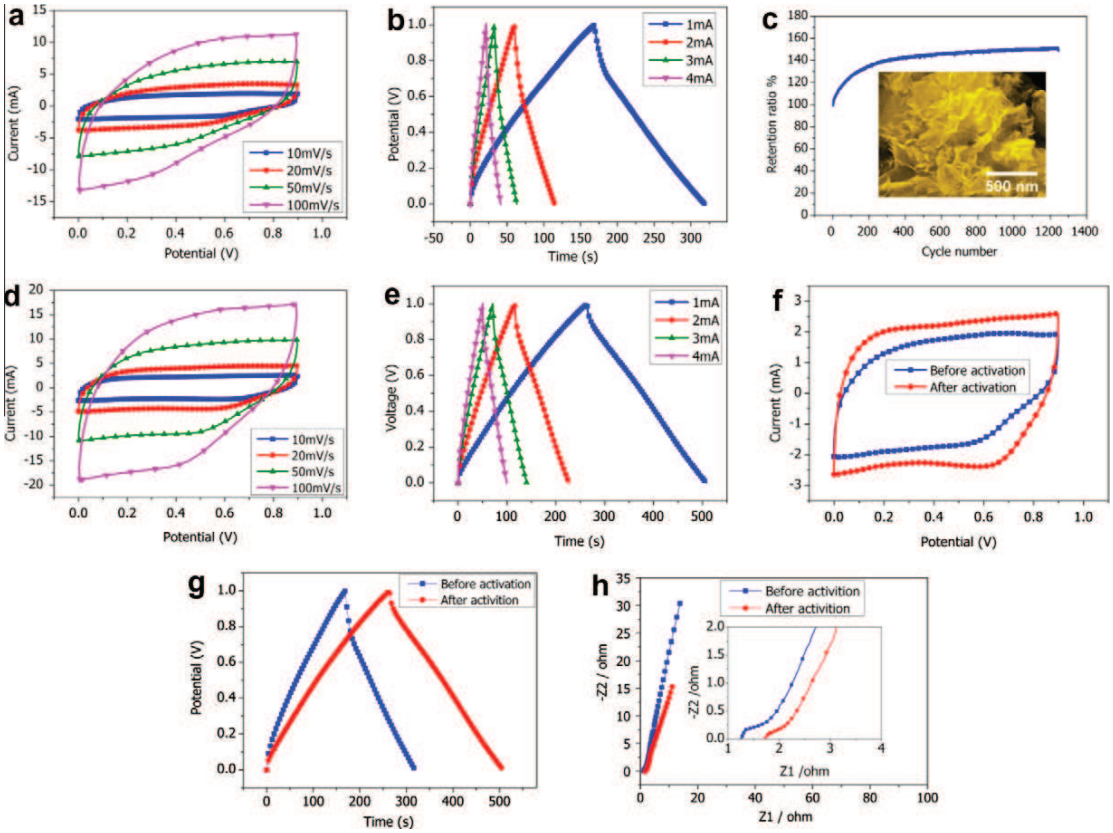

Fig. 4 – Electrochemical measurement of graphene electrode. (a) CV curves of the graphene electrode at different scan rates from 10 to 100 mV/s. (b) Charge and discharge curves of the graphene electrode at different charging current from 1 to 4 mA. (c) Electro-activation of graphene electrode. The SEM image below the curve is the morphology of the graphene after activation. There is no noticeable morphological difference after electro-activation. (d) CV curves of graphene after activation at scan rates from 10 to 100 mV/s. (e) Charge and discharge curves of the graphene electrode after activation at different charging current from 1 to 4 mA. (f) Comparison of CV curves before and after electro-activation. (g) Comparison of charge and discharge curves before and after electro-activation. (h) Nyquist plot of the graphene electrode before and after electro-activation. Inset is a magnified portion of the plot near the origin.

of electro-activation without charging any current for comparison, but the specific capacitance did not change, which confirmed our suggestion that "electro-activation" is truly operational for improving the performance of the pure graphene supercapacitor.

From the CV curves obtained after electro-activation, it revealed that the shape of the curves is very much like the one before activation as shown in Fig. 4d. But the platform current increased a lot, indicating an increase of specific capacitance. It was also confirmed by the charge and discharge curves which are showed in Fig. 4d. The specific capacitance calculated by the charge and discharge curve after electro-activation is 245 F/g and it is enhanced by more than 60% comparing to the one before electro-activation. The corresponding energy density is 8.5 Wh/kg. The CV curves before and after electro-activation are shown in Fig. 4e at the scan rate of 10 mA/s. The current increased a lot, indicating a larger capacitance. Furthermore, the shape of the curve looks more rectangular. This is attributed to a better wettability after electro-activation. The comparison of charge and discharge curves also confirmed that the electrode after electro-activation has a longer charging time which also means a larger capacitance (Fig. 4f).

The specific capacitance of 245 F/g is much higher than those of CNT-based supercapacitors reported the literature, 102 and 180 F/g, respectively [44,45]. The graphene-based supercapacitor showed a higher specific capacitance is likely due to the fact that the graphene nano-sheets can move physically to adapt different electrolyte ions, leading to a higher accessibility of electrolyte ions and also a more effective use of the specific surface area [6].

The use of a complex-plane plot, or Nyquist plot, to represent the impedance behavior as a function of frequency has often been used to evaluate the frequency response of supercapacitors. In the complex-plane, the imaginary component, Z_2, is usually used to represent the capacitive parameter and the Z_1 (the real component) represents the ohmic parameter. The two components are all studied under a certain frequency range. This kind of plots usually consists of one or more semicircles in the complex plane, sometimes with the center of a semicircle depressed below the Z_1 axis. The theoretical Nyquist plot of a supercapacitor consists of three regions which are dependent on the frequencies. At very high frequency, the supercapacitor behaves like a pure resistor. At low frequency, the imaginary part sharply increases and a vertical line is usually observed, indicating a pure capacitive behavior. In the middle frequency domain, the influence of the electrode porosity can be observed. When the frequency decreases, starting from the very high frequency, the signal penetrates deeper and deeper inside the porous structure of the electrode, then more and more electrode surface becomes available for ion adsorption. This middle frequency range is related to the electrolyte penetration inside the porous structure of the high porosity electrodes and this region is usually called the Warburg curve [46]. Fig. 4h is the Nyquist plot of the pure graphene electrode before and after electro-activation. Both of the curves appear as straight lines at low frequency and an arc in the high frequency region. The high frequency loops of before and after the activation are 8414 to 75 Hz and 5623 to 96 Hz, respectively. This loop shift is related to the electrical resistance between the graphene nanosheets. The semi-circle loop has been observed and reported in carbon-based supercapacitors by numerous authors in the literature. It usually finds a very big loop in activated carbon electrode supercapacitors which means a large inter-granular electrical resistance between the activated carbon particles. It largely depends on the electrode surface area and the inter-particle resistivity. The realization of thin active layers or adding some low surface area conductive additives can reduce this value, but will lead to a low capacitance per area or capacitance per weight. The loop may also have some relationship between the active material and the current collector. The small loop regions in Fig. 4h show a low electrical resistance between the graphene nanosheets and good conductivity of between the graphene electrode and current collector. The Warburg curve in Fig. 4h is very short, indicating a good access of electrolyte ions to the graphene surface. The equivalent series resistance (ESR) is obtained from the x-intercept of the Nyquist plot in Fig. 4h. They are 1.25 and 1.73 Ω, respectively. ESR data determine the rate that the supercapacitor can be charged and discharged, and it is a very important factor to determine the power density of a supercapacitor.

The specific power density before and after the electro-activation are the 50 and 36.1 kW/kg, respectively. This high value of power density promises that such supercapacitors can be used in surge-power delivery applications.

Fig. 5 gives schematic illustrations and an SEM image of the MnO_2-coated graphene electrode to explain why the MnO_2 coated graphene electrodes have outstanding performance. Fig. 5a is a schematic before and after MnO_2 electroposition. The MnO_2 nanoflowers were grown on both sides of the graphene nanosheets to form a very unique electrode structure. The ion diffusion rate would be enhanced in this structure since the distance between graphene sheets could

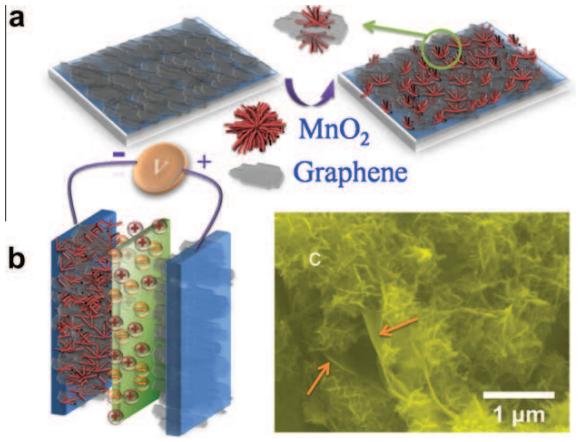

Fig. 5 – Schematics illustrating coating of graphene with MnO_2 nanoflowers. (a) Schematic of the graphene electrode and the MnO_2-coated graphene electrode. (b) Schematic of asymmetric supercapacitor with graphene as anode and MnO_2-coated graphene as cathode. (c) SEM image of the MnO_2-coated graphene. It also shows the graphene nanosheets which are indicated by arrows.

increase due to growing the MnO_2 nanostructures. We assembled our test cell as an asymmetric supercapacitor with graphene as the anode and MnO_2-coated graphene as the cathode as shown schematically in Fig. 5b. We also offered further evidence in the SEM image in Fig. 5c that the MnO_2 nanoflowers were grown indeed on the surface of the graphene nano-sheets.

Fig. 6a and b show the CV curves and the charge and discharge curves after MnO_2 coating under different scan rates and charging currents. The shape of CV plot, nearly rectangular with mirror symmetry, did not change much in all of the applied scan rates compared to the pure graphene electrode before MnO_2 coating, which indicates an excellent reversibility and ideal capacitive property of the electrode. The CV curves before and after MnO_2 coating at the scan rate of 10 mV/s is given in Fig. 6c. The current increased a lot after coating. It is believed that the increase of current is due to the redox reactions of MnO_2 which is coated on the graphene. It has been reported that the pseudocapacitance of MnO_2 in aqueous neutral electrolytes could be attributed to the following redox reaction:

$$MnO_2 + \delta X^+ + \delta e^- \leftrightarrow MnOOX_\delta,$$

where X^+ corresponds to H^+ or alkali metal cations such as Na^+ and K^+. On the basis of Faraday's law, the theoretical specific capacitance of the reduction of $Mn(IV)O_2$ to $Mn(III)OO_X$ is approximately 1100 F/g with a voltage window of 1.0 V [47]. The charging and discharging curves under 1 mA of the electrode before and after MnO_2 coating are shown in Fig. 6d. Both charge and discharge times increased after the MnO_2 coating. The supercapacitor test cell is assembled as a two-electrodes system which uses the pure graphene as the anode and the MnO_2-coated graphene as the cathode. The calculated specific capacitance after the MnO_2 coating is 328 F/g. The specific capacitance increased 34.4% after the MnO_2 coating. The energy density after the MnO_2 coating can reach to 11.4 Wh/kg. Fig. 6e shows the Nyquist plots of the MnO_2-coated graphene electrode. The ERS is 2.2 Ω which is calculated from the x-intercept on the plot. The maximum power density is 25.8 kW/kg. The high frequency loop is from 2371 to 14 Hz. The loop is quite small, indicating a small resistance between graphene and the MnO_2 nanostructures. This is because the nanostructured MnO_2 is grown on the graphene sheets electrochemically rather than a mechanical blending. We could also find in the Nyquist plot that the MnO_2-coated graphene has more straight line than the pure graphene electrode in the low frequency region. Since an ideally polarizable capacitance gives rise to a straight vertical line along the series, this line must have a finite slope to represent the diffusive resistance of electrolyte in the electrode pores and the proton diffusion in host materials. Generally this type of proton diffusion (solid-state diffusion) is slower in host materials than in electrolyte, therefore, the linearity is assumed to be the semi-infinite diffusion in solid materials. The slope of the MnO_2-coated graphene increased due to a lowered diffusion resistance by the shortened proton diffusion path. The in situ electrochemical coating is a three-dimensional coating of the entire graphene electrode. The growth of the MnO_2 nanostructures could therefore broaden the distance between the graphene nanosheets, which would then to make it easier for electrolyte ion transfer. The long time cycling is shown in Fig. 6f. We found that the capacitance increased at the beginning of the cycling just like the pure graphene electrodes. However, it kept almost as a constant after about 150 cycles,

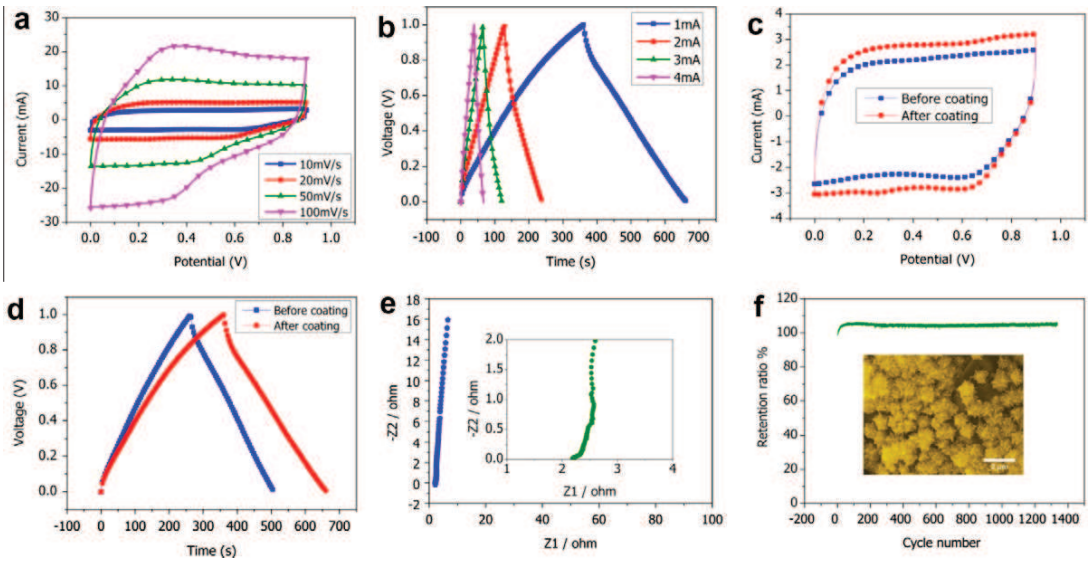

Fig. 6 – Electrochemical properties of graphene electrode after MnO_2 coating. (a) CV curves of MnO_2-coated graphene electrode at different scan rates from 10 to 100 mV/s. (b) Charge and discharge curves of MnO_2-coated graphene electrode at different charging current from 1 to 4 mA. (c) Comparison of CV curves before and after MnO_2 coating. (d) Comparison of charge and discharge curves before and after MnO_2 coating. (e) Nyquist plot of MnO_2-coated graphene electrode. Inset is a magnified portion of the plot near the origin. (f) Capacitance retention curve in aqueous electrolyte. The image below the retention curve shows the SEM morphology after aging.

the capacitance only dropped by 1% after 1300 cycles, indicating an excellent cyclicity of the MnO_2-coated graphene electrode.

The graphene and MnO_2-coated graphene both showed very good power and energy performance. The outstanding properties are attributed to the high accessible specific surface area and high efficiency of electrolyte ion absorption. Graphene sheets with either individual single-layered sheet or few-layered graphite can offer an ideal structure for ion absorption. Moreover, the graphene-based electrode does not depend on the exact pore distribution in its solid support to provide its large surface area. The graphene nano-sheet can adjust automatically to different types of electrolyte. Thus, access to the very high surface area of graphene materials by the electrolyte can be maintained while preserving the overall high electrical conductivity. The graphene based electrode can have a larger thickness than the activated carbon-based electrode, which could therefore offer a higher capacitance per area. That is because activated carbon has a higher electrical resistance which limits the thickness and usually contains conductive but low surface area additives such as carbon black to enable rapid electrical charge transfer from the cell [6]. The high electrical conductivity of the graphene materials eliminates the need for conductive fillers and thus allows an increased electrode thickness. Increasing the electrode thickness and elimination additives lead to improved electrode materials for collection/separation, which would in turn further increase the energy density of the supercapacitor. The MnO_2 nanoflowers which are grown on every graphene nano-sheet can enlarge the distance between the graphene sheets to increase the access of the electrolyte ions. It has been reported that the MnO_2 nanostructures can only have the surface layer or some nanometers thickness can attend the redox reactions with the cations in the electrolyte. So the nano-structure MnO_2 could have good efficiency to have redox reactions and further increased the specific capacitance. So the high performance of the supercapacitor electrode benefits from both graphene and nano-structured MnO_2.

Our MnO_2-coated graphene electrodes have a high specific capacitance and excellent power performance, which suggested a high potential for applications in hybrid vehicles as energy saving components. Nickel metal hydride (NiMH) battery which is frequently used in the hybrid vehicles has some drawbacks such as limited service life, limited discharge current, high self-discharge, and poor temperature adaption. The graphene based supercapacitor can surely solve these problems without losing its performance. Therefore the supercapacitors can be used as the electric energy storage device for the hybrid vehicles.

4. Conclusions

In summary, we have successfully fabricated binderless supercapacitors using graphene and MnO_2-nanoflowers coated graphene to provide a high specific capacitance of 245 F/g for graphene and 328 F/g for MnO_2-coated graphene. The electrodeposited γ-MnO_2 is suggested to serve as a spacer to increase the ion diffusion rate in the electrolyte. The surface decoration of graphene can increase greatly the energy density of the supercapacitor, which makes the supercapacitor possible to use in the hybrid vehicles or pure electrical vehicles. We also found that the electro-activation is an effective way to activate the potential of graphene-based electrode. What is more, the power density of our asymmetric supercapacitor reached 25.8 kW/kg, which is well suited for high power applications. The MnO_2 nanoflowers coated on graphene make it quite a promising material as a high energy and high power density electrode for supercapacitors. Furthermore, the results are also potentially useful for preparation of other graphene-based composite films with varied properties in order to meet diverse applications, such as lithium ion batteries, electrochemical sensor and solar cells.

Acknowledgments

This work was supported by JSPS Grants-in-Aid for Scientific Research Nos. 19310081 and 22310074, and the "Nanotechnology Network Project" of the Ministry of Education, Culture, Sports, Science and Technology (MEXT), Japan.

REFERENCES

[1] Simon P, Gogotsi Y. Materials for electrochemical capacitors. Nat Mater 2008;7(11):845–54.
[2] Frackowiak E, Beguin F. Carbon materials for the electrochemical storage of energy in capacitors. Carbon 2001;39(6):937–50.
[3] Frackowiak E, Beguin F. Electrochemical storage of energy in carbon nanotubes and nanostructured carbons. Carbon 2002;40(10):1775–87.
[4] Futaba DN, Hata K, Yamada T, Hiraoka T, Hayamizu Y, Kakudate Y, Tanaike O, Hatori H, Yumura M, Iijima S. Shape-engineerable and highly densely packed single-walled carbon nanotubes and their application as super-capacitor electrodes. Nat Mater 2006;5(12):987–94.
[5] Wang Y, Shi ZQ, Huang Y, Ma YF, Wang CY, Chen MM, Chen YS. Supercapacitor devices based on graphene materials. J Phys Chem C 2009;113(30):13103–7.
[6] Stoller MD, Park SJ, Zhu YW, An JH, Ruoff RS. Graphene-based ultracapacitors. Nano Lett 2008;8(10):3498–502.
[7] Wang DW, Li F, Zhao JP, Ren WC, Chen ZG, Tan J, Wu ZS, Gentle I, Lu GQ, Cheng HM. Fabrication of graphene/polyaniline composite paper via in situ anodic electropolymerization for high-performance flexible electrode. ACS Nano 2009;3(7):1745–52.
[8] Fischer AE, Pettigrew KA, Rolison DR, Stroud RM, Long JW. Incorporation of homogeneous, nanoscale MnO_2 within ultraporous carbon structures via self-limiting electroless deposition: implications for electrochemical capacitors. Nano Lett 2007;7(2):281–6.
[9] Chang JK, Lee MT, Tsai WT, Deng MJ, Cheng HF, Sun IW. Pseudocapacitive mechanism of manganese oxide in 1-ethyl-3-methytimidazolium thiocyanate ionic liquid electrolyte studied using X-ray photoelectron spectroscopy. Langmuir 2009;25(19):11955–60.
[10] Conway BE. Transition from supercapacitor to battery behavior in electrochemical energy-storage. J Electrochem Soc 1991;138(6):1539–48.
[11] Long JW, Swider KE, Merzbacher CI, Rolison DR. Voltammetric characterization of ruthenium oxide-based

aerogels and other RuO_2 solids: the nature of capacitance in nanostructured materials. Langmuir 1999;15(3):780–5.
[12] Frackowiak E, Khomenko V, Jurewicz K, Lota K, Beguin F. Supercapacitors based on conducting polymers/nanotubes composites. J Power Sources 2006;153(2):413–8.
[13] Ryu KS, Kim KM, Park NG, Park YJ, Chang SH. Symmetric redox supercapacitor with conducting polyaniline electrodes. J Power Sources 2002;103(2):305–9.
[14] Khomenko V, Frackowiak E, Beguin F. Determination of the specific capacitance of conducting polymer/nanotubes composite electrodes using different cell configurations. Electrochim Acta 2005;50(12):2499–506.
[15] Park JH, Ko JM, Park OO, Kim DW. Capacitance properties of graphite/polypyrrole composite electrode prepared by chemical polymerization of pyrrole on graphite fiber. J Power Sources 2002;105(1):20–5.
[16] Kotz R, Carlen M. Principles and applications of electrochemical capacitors. Electrochim Acta 2000;45(15-16):2483–98.
[17] Shaijumon MM, Ou FS, Ci LJ, Ajayan PM. Synthesis of hybrid nanowire arrays and their application as high power supercapacitor electrodes. Chem Commun 2008;20:2373–5.
[18] Meyer JC, Geim AK, Katsnelson MI, Novoselov KS, Booth TJ, Roth S. The structure of suspended graphene sheets. Nature 2007;446(7131):60–3.
[19] Gomez-Navarro C, Weitz RT, Bittner AM, Scolari M, Mews A, Burghard M, Kern K. Electronic transport properties of individual chemically reduced graphene oxide sheets. Nano Lett 2007;7(11):3499–503.
[20] Becerril HA, Mao J, Liu Z, Stoltenberg RM, Bao Z, Chen Y. Evaluation of solution-processed reduced graphene oxide films as transparent conductors. ACS Nano 2008;2(3):463–70.
[21] Tung VC, Allen MJ, Yang Y, Kaner RB. High-throughput solution processing of large-scale graphene. Nat Nanotechnol 2009;4(1):25–9.
[22] Stankovich S, Dikin DA, Dommett GHB, Kohlhaas KM, Zimney EJ, Stach EA, Piner RD, Nguyen ST, Ruoff RS. Graphene-based composite materials. Nature 2006;442(7100):282–6.
[23] Geim AK, Kim P. Carbon wonderland. Sci Am 2008;298(4):90–7.
[24] Shinomiya T, Gupta V, Miura N. Effects of electrochemical-deposition method and microstructure on the capacitive characteristics of nano-sized manganese oxide. Electrochim Acta 2006;51(21):4412–9.
[25] Cheng L, Li HQ, Xia YY. A hybrid nonaqueous electrochemical supercapacitor using nano-sized iron oxyhydroxide and activated carbon. J Solid State Electr 2006;10(6):405–10.
[26] Thackeray MM. Manganese oxides for lithium batteries. Prog Solid State Chem 1997;25(1–2):1–71.
[27] Ammundsen B, Paulsen J. Novel lithium-ion cathode materials based on layered manganese oxides. Adv Mater 2001;13(12–13):943.
[28] Whittingham MS. Lithium batteries and cathode materials. Chem Rev 2004;104(10):4271–301.
[29] Pang SC, Anderson MA, Chapman TW. Novel electrode materials for thin-film ultracapacitors: comparison of electrochemical properties of sol–gel-derived and electrodeposited manganese dioxide. J Electrochem Soc 2000;147(2):444–50.
[30] Lee HY, Kim SW, Lee HY. Expansion of active site area and improvement of kinetic reversibility in electrochemical pseudocapacitor electrode. Electrochem Solid State 2001;4(3):A19–22.
[31] Chin SF, Pang SC, Anderson MA. Material and electrochemical characterization of tetrapropylammonium manganese oxide thin films as novel electrode materials for electrochemical capacitors. J Electrochem Soc 2002;149(4):A379–84.
[32] Miura N, Oonishi S, Prasad KR. Indium tin oxide/carbon composite electrode material for electrochemical supercapacitors. Electrochem Solid State 2004;7(8):A247–9.
[33] Prasad KR, Miura N. Electrochemically synthesized MnO_2-based mixed oxides for high performance redox supercapacitors. Electrochem Commun 2004;6(10):1004–8.
[34] Xiong YJ, Xie Y, Li ZQ, Wu CZ. Growth of well-aligned gamma-MnO_2 monocrystalline nanowires through a coordination-polymer-precursor route. Chem-Eur J 2003;9(7):1645–51.
[35] Subramanian V, Zhu HW, Vajtai R, Ajayan PM, Wei BQ. Hydrothermal synthesis and pseudocapacitance properties of MnO_2 nanostructures. J Phys Chem B 2005;109(43):20207–14.
[36] Sugantha M, Ramakrishnan PA, Hermann AM, Warmsingh CP, Ginley DS. Nanostructured MnO_2 for Li batteries. Int J Hydrogen Energ 2003;28(6):597–600.
[37] Tench D, Warren LF. Electrodeposition of conducting transition-metal oxide hydroxide films from aqueous-solution. J Electrochem Soc 1983;130(4):869–72.
[38] Moore GJ, Portal R, La Salle ALG, Guyomard D. Synthesis of nanocrystalline layered manganese oxides by the electrochemical reduction of AMnO(4) (A = K, Li). J Power Sources 2001;97(8):393–7.
[39] Ghaemi M, Biglari Z, Binder L. Effect of bath temperature on electrochemical properties of the anodically deposited manganese dioxide. J Power Sources 2001;102(1–2):29–34.
[40] Yan J, Fan ZJ, Wei T, Qian WZ, Zhang ML, Wei F. Fast and reversible surface redox reaction of graphene–MnO_2 composites as supercapacitor electrodes. Carbon 2010;48(13):3825–33.
[41] Wu ZS, Ren W, Wang DW, Li F, Liu B, Cheng HM. ACS Nano 2010;4(10):5835–42.
[42] Liu R, Lee SB. MnO_2/poly(3,4-ethylenedioxythiophene) coaxial nanowires by one-step coelectrodeposition for electrochemical energy storage. J Am Chem Soc 2008;130(10):2942–3.
[43] Qu DY. Studies of the activated carbons used in double-layer supercapacitors. J Power Sources 2002;109(2):403–11.
[44] Niu CM, Sichel EK, Hoch R, Moy D, Tennent H. High power electrochemical capacitors based on carbon nanotube electrodes. Appl Phys Lett 1997;70(11):1480–2.
[45] An KH, Kim WS, Park YS, Moon JM, Bae DJ, Lim SC, Lee YS, Lee YH. Electrochemical properties of high-power supercapacitors using single-walled carbon nanotube electrodes. Adv Funct Mater 2001;11(5):387–92.
[46] Portet C, Taberna PL, Simon P, Laberty-Robert C. Modification of Al current collector surface by sol–gel deposit for carbon–carbon supercapacitor applications. Electrochim Acta 2004;49(6):905–12.
[47] Ma SB, Nam KW, Yoon WS, Yang XQ, Ahn KY, Oh KH, Kim KB. Electrochemical properties of manganese oxide coated onto carbon nanotubes for energy-storage applications. J Power Sources 2008;178(1):483–9.